VIP *Very Important Paper*

Effects of I_3^- Electrolyte Additive on the Electrochemical Performance of Zn Anodes and Zn/MnO_2 Batteries

Siying Liu[+],[a] Wenshuo Shang[+],[a] Yaxin Yang,[a] Dongjian Kang,[a] Changsheng Li,[a] Buting Sun,[a] Litao Kang,*[a] Shan Yun,[b] and Fuyi Jiang*[a]

While delivering the highest energy density among low-cost aqueous batteries, the practical implement of rechargeable Zn-ion batteries (ZIBs) is still seriously restricted by the dynamic parasitic reactions on the metallic Zn anodes including dendrite growth, H_2 evolution and corrosion reactions. Modulating electrolyte is identified as a facile and effective approach to restrain these detrimental processes by various chemical mechanisms. Herein, we report a new strategy to improve the performance of Zn anodes and ZIBs by simply adding I_3^- species into the electrolytes. The I_3^- can react with the surface Zn and passivate the growth hotspots of Zn dendrites, prolonging the cycling lifetime of the electrodes. As a competitive reaction, it can also suppress the H_2O-derived corrosion and H_2 evolution process. The I_3^- is regenerable by oxidizing reactions on cathode surface, and can therefore long-term persist its beneficial effects in ZIBs, as demonstrated in the classic Zn/MnO_2 battery. However, the I_3^- additive seems failed in evolving into a dense interfacial protective layer, and may be useful as a supplementary measure to prevent shorting failure of Zn-based batteries.

1. Introduction

Thanks to its remarkable advantages including low cost, high capacity (5855 mAh cm^{-3} or 820 mAh g^{-1}), abundant resource, environmental benignity, low redox potential (−0.76 eV vs. SHE) and decent aqueous compatibility,[1] Zn becomes not only the anode of the historic "voltaic pile", but also one of the rare metallic anodes successfully commercialized in primary batteries.[2] When it comes to rechargeable batteries, nevertheless, the repeated Zn striping/plating process remarkably accelerates dendritic growth and parasitic reactions such as H_2 evolution and corrosion reactions, resulting in poor cycling stability and short lifetime due to metallic Zn consumption and short-circuit failure.[1a] Therefore, converting the Zn-based primary batteries into robust rechargeable ones remains yet a substantial challenge.[1c,3]

Adopting thermodynamically stable organic electrolytes is a straightforward approach to circumvent the detrimental parasitic reactions of Zn-ion batteries (ZIBs).[4] In organic electrolytes with base solvents of acetonitrile, diglyme, propylene carbonate, or N, N-dimethylformamide, high Zn striping/plating coulombic efficiencies $\geq$99% can be easily achieved, due to the intrinsic stability of metallic Zn in these water-free media.[5] The adoption of organic electrolytes is also helpful to widen the ZIBs' operation voltages.[6] Nevertheless, water is an indispensable assistance for the smooth occurrence of most cathodic reactions of ZIBs.[7] It means that electrochemical performances of most ZIBs' cathode materials will dramatically deteriorate in pure organic electrolytes.[7c,8] This fact significantly increases the importance of developing Zn-stabilizing strategies in aqueous electrolytes.[9]

Inspired by the SEI layers in lithium-ion batteries (LIBs),[10] a mainstream strategy of pre-constructing artificial SEI layers on Zn anodes is introduced to protect Zn anodes of ZIBs. The studied artificial SEI layers including polyamide/Zn(OTf)$_2$,[11] PVB,[12] montmorillonite/PVDF,[13] ZnF_2,[14] ZnS,[15] and ZnSe[16] coatings, to name only a few. These layers show impressive suppressibility to parasitic reactions while ensuring uniform Zn plating.[3,17] The main drawback of this strategy is the lack of repairability of these artificial SEI layers,[18] i.e., the functions of these layers will deteriorate once penetrating cracks and/or scratches formed.[19]

Rational electrolyte design is another appealing strategy to protect metallic anodes including Zn.[20] Interestingly, the underneath principles of electrolyte design are very diverse. For example, in "water-in-salt"[21] and "water-in-deep eutectic solvent (water-in-DES)"[22] electrolytes, all water molecules participate into the salt's or DES's internal interaction networks by H-bonding and coordinating, by which the free-water-content and the related parasitic reactions are remarkably suppressed. Hydrogel electrolytes with thickening agents can also alleviate the parasitic reactions by confine most of the free-water away from electrolyte/electrode interfaces, along with homogenizing Zn^{2+} flux for uniform Zn plating.[23] Some surfactants or cations, on the other hand, can improve the

[a] S. Liu,[+] W. Shang,[+] Y. Yang, D. Kang, C. Li, B. Sun, Prof. Dr. L. Kang, Prof. Dr. F. Jiang
College of Environment and Materials Engineering
Yantai University
Yantai 264005, China
E-mail: kanglitao@ytu.edu.cn
fyjiang@ytu.edu.cn
[b] Dr. S. Yun
Faculty of Chemical Engineering
Huaiyin Institute of Technology
Huai'an 223003, China

[+] *These authors contributed equally to this work.*

Supporting information for this article is available on the WWW under https://doi.org/10.1002/batt.202100221

nucleation and growth uniformity of the plated Zn, mainly by surficial absorption[24] and electrostatic repulsion,[25] similar to the role played by potassium perfluorinated sulfonates in LIBs' electrolytes.[20] Modulating the zinc salts[26] or solvated shells of Zn^{2+} with electrolyte additives has also proven effective to optimize the Zn striping/plating behaviors of metallic Zn anodes. In this regard, well established additives include, at least, dimethyl sulfoxide,[27] ethylene glycol,[28] dimethyl carbonate[29] and diethyl ether.[30] Recently, researchers further reveal the effectiveness of electrolyte additives on in-situ constructing artificial SEI layers on Zn anodes,[1b,18, 31] for example, $Zn(NO_3)_2$ or $Zn(H_2PO_4)_2$ in $Zn(CF_3SO_3)_2$ (i.e., $Zn(OTf)_2$) aqueous electrolytes to facilitate the formation of organic-terminated $Zn_5(CO_3)_2(OH)_6/ZnF_2$[18] or $Zn_3(PO_4)_2\cdot 4H_2O$ SEI layer.[18]

Significantly, the I^-/I_3^- couple holds a proper redox potential and superb cycling durability in both aqueous and organic electrolytes.[32] Besides working as the cathode active material in Zn-iodine flow batteries, I_3^- is also a common intermediate discharge product of all iodine batteries, due to the coordination between solid I_2 cathode with its discharge product I^-. The highly soluble I_3^- can easily penetrate through porous battery separators, and cause fast self-discharge.[33] Interestingly, the oxidizing I_3^- has also been intelligently used to scavenge the Zn dendrites filled in the separator membranes via redox reaction, in order to avoid micro-short-circuiting.[34] In the outstanding works by Jin et al.,[35] proper amount of I_3^- additive was deliberately introduced into the electrolyte of Li-metal batteries, which can effectively retrieve and rejuvenate the trapped Li species in both dead Li dendrites (i.e., electrically isolated Li debris) and discarded SEI by converting it into solvable Li^+.

In this work, we investigate the influences of I_3^- electrolyte additive on the performances of both Zn anodes and ZIBs. It is found that the oxidizing I_3^- cations can react with the metallic Zn and thereby passivate the growth hotspots of Zn dendrites. The above reaction also modifies the H_2O-derived corrosion process and the morphology of side product $Zn_4(OH)_6SO_4\cdot H_2O$ as a competitive reaction. With the I_3^- additive in electrolytes, the cycling stability of both Zn anodes and Zn/MnO_2 batteries can be dramatically prolonged, with only slight increase of self-discharge. This method is applicable to cheap $ZnSO_4$ electrolytes, very helpful to retain the cost competitiveness of ZIBs. In addition, the findings of this work may also provide insights for the rational design of iodine-cathode batteries.

2. Results and Discussion

Figure 1a,b depict the absorption spectra and optical images (insets) of the control- and I- (i.e., I_3^--containing) electrolytes before and after Zn foil immersion. The pristine I-electrolyte demonstrates a maroon color, because of the distinct absorption bands of I_3^- centering at 288 and 354 nm (Figure 1a).[35,36] After Zn immersion, these I_3^- absorption bands disappear and the electrolyte turns into colorless (Figure 1b), suggesting the

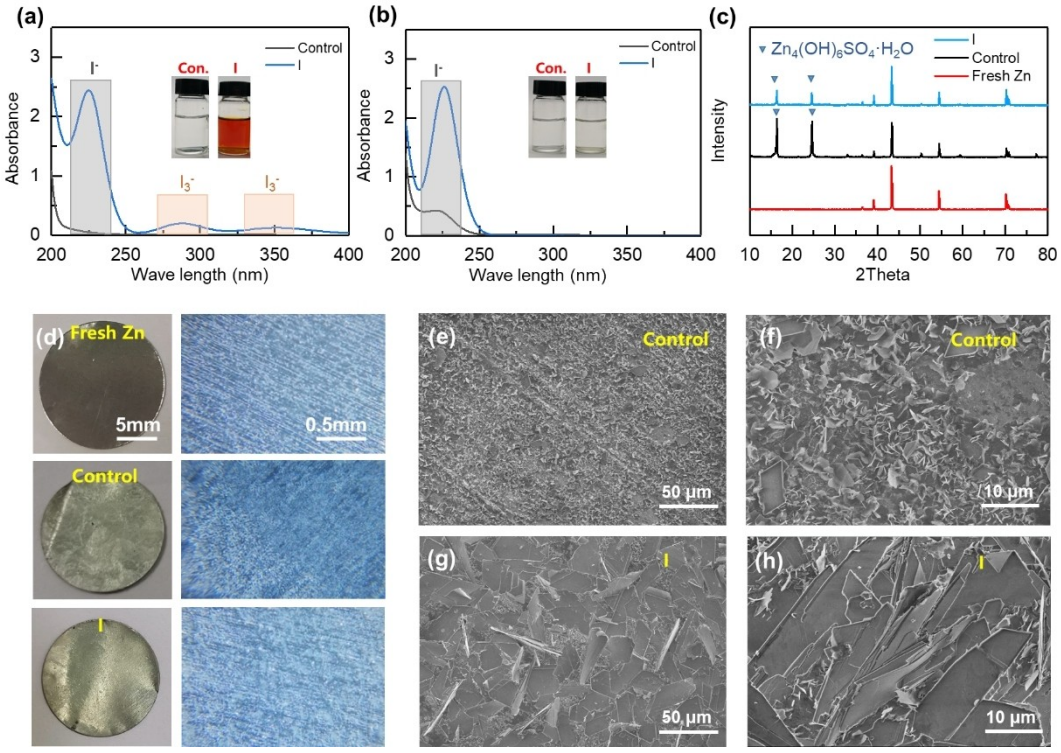

Figure 1. UV-vis absorption spectra of the control- and I-electrolytes: a) before and b) after Zn foils immersion for 48 h. The insets show the optical images of corresponding electrolytes. c) XRD patterns, d) optical images of fresh and treated Zn foils immersed in control- and I-electrolytes for 48 h. e–h) SEM images of Zn foils immersed in difference electrolytes.

occurrence of redox reaction between the oxidizing I_3^- and the metallic Zn, as expressed below:[34]

$$I_3^- + Zn \rightarrow Zn^{2+} + 3I^- \quad (1)$$

This reaction competes with the H_2O-derived Zn corrosion process [Eq. (2)],[23b,37] and thus helps to suppress the Zn corrosion, H_2 evolution, as well as $Zn_4(OH)_6SO_4 \cdot H_2O$ formation. The lower corrosion trend of Zn foils in the I-electrolyte is also confirmed by Tafel curves (Figure S1). As a result, the Zn foil immersed in the I-electrolyte generates a much lower content of $Zn_4(OH)_6SO_4 \cdot H_2O$ than the one in control-electrolyte (Figure 1c).

$$4Zn + SO_4^{2-} + 9H_2O \rightarrow Zn_4(OH)_6SO_4 \cdot H_2O + 2OH^- + 4H_2\uparrow \quad (2)$$

At the same time, the morphology of $Zn_4(OH)_6SO_4 \cdot H_2O$ layers formed in the electrolytes are also modified by the I_3^- additive (Figure 1d). Microscopically, the $Zn_4(OH)_6SO_4 \cdot H_2O$ formed in the I-electrolyte are much larger and more parallel to the underneath Zn foil (Figure 1e–h), possibly due to the increased Zn^{2+} supply in the vicinity of the Zn foil's surfaces by [Eq. (1)].[38] It is widely reported that electrochemically-inert covering layers on Zn anodes can protect separators from piercing, and thus stabilize batteries and prolong their lifetime.[14a,39] Moreover, the addition of I_3^- species improves wettability of the electrolyte on Zn foils (Figure S2), which should also be favorable to improve Zn striping/plating uniformity.[38,40]

The effectiveness of the I-electrolyte on stabilizing Zn plating-striping reactions can be clearly revealed by the galvanostatic cycling test of Zn/Zn symmetric cells in different electrolytes. As shown in Figure 2a, both cells deliver comparable striping/plating overpotentials of ~35 mV at the beginning. The overpotential of the control-cell keeps relatively stable within the first 225 h (35–40 mV), and then a sudden and slight drop (down to ~29 mV) happens between 225~243 h, possibly because of soft short-circuit caused by the recoverable local contact.[16] Afterwards, the curve becomes very unstable with fluctuating overpotentials (30~350 mV) until the final irreversible hard short-circuit failure at 1277 h, indicating an uneven Zn striping/plating process.[16] In contrast, the I-electrolyte endows the cell with an ultralong cycling lifespan of over 1430 h, along with a small and stable overpotential lower than 40 mV in the entire cycling process, thanks to the larger exchange current densities (2.72 vs. 1.13 $\mu A\,cm^{-2}$, Figure S1) and faster Zn deposition kinetics in this electrolyte. Similar phenomenon is highly reproducible in Zn/Zn symmetric cells cycling at a wide range of current densities and areal capacities (Figure 2b and S3). At even a high depth of discharge (DOD) of 34% (4 $mAh\,cm^{-2}$, Zn foil thickness: 20 μm), the I-electrolyte cell works still well within a test period of 40 h. By comparison, the control-cell failed after only 17 h under the same testing condition. Postmortem examinations indicate that both Zn anodes were covered by a rough layer of $Zn_4(OH)_6SO_4 \cdot H_2O$ (Figure 2c–e).

In Zn/Zn symmetric cells, the I_3^- anions should be quickly reduced into I^- by the Zn electrodes after device assembly (Figure 1a,b). It means that the influence of these oxidizing I_3^- species should mainly exists at the first few cycles. Surprisingly, the I-electrolyte can still endow the Zn/Zn symmetric cells with an obvious and even long-term stability. To clarify this puzzle, two control experiments were performed on Zn/Zn symmetric cells with either fresh Zn electrodes in $KI + ZnSO_4$ electrolyte (labeled as: Fresh $Zn + ZnSO_4 + KI$) or I_3^--pretreated Zn electrodes in $ZnSO_4$ electrolyte (I_3^--pretreated $Zn + ZnSO_4$). As shown in Figure 3a, the fresh $Zn + ZnSO_4 + KI$ cell failed after 180 h, while the cell with I_3^--pretreated Zn electrodes still works even

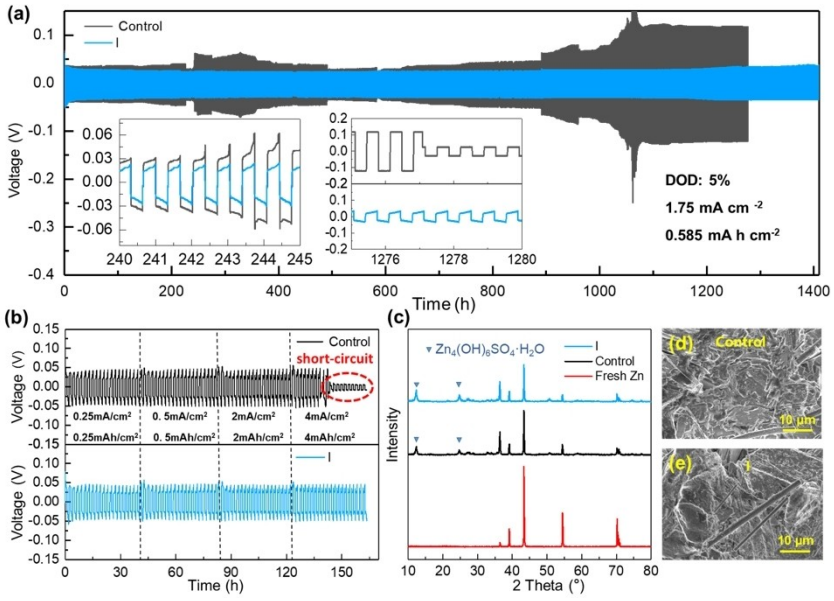

Figure 2. a, b) The voltage profiles of Zn/Zn symmetric cells with either control- or I-electrolyte in galvanostatic cycling test. c) XRD patterns and d, e) SEM images of the cycled Zn anodes after 1430 h cycling test as shown in panel (a).

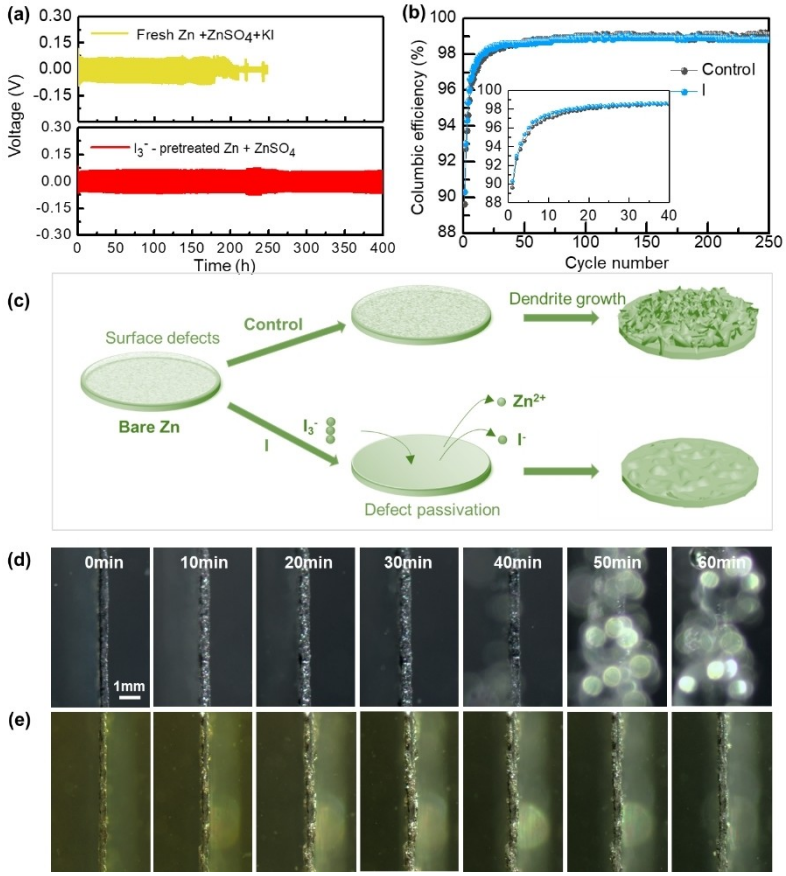

Figure 3. a) The voltage profiles of Zn/Zn symmetric cells with either fresh Zn in KI + $ZnSO_4$ electrolyte (labeled as: Fresh Zn + $ZnSO_4$ + KI) or I_3^--pretreated Zn in $ZnSO_4$ electrolyte (I_3^--pretreated Zn + $ZnSO_4$); b) Coulombic efficiencies (CEs) of Zn/Cu symmetric cells in either control- or I-electrolyte at a current density of 0.25 mA cm^{-2}. c) Schematic illustration showing the effects of the I_3^- additive on Zn electrodes' striping/plating process. Optical micrographs of Zn^{2+} deposition behavior in: d) control- and e) I-electrolyte. Thicker Zn foils were employed in this test, because the 20 μm thick foils are too flexible for stable observation.

after 400 h, with only a slight increase of overpotential from approximately 52 to 65 mV. Due to the beneficial impacts of the I_3^- species, the Zn/Cu asymmetric cells achieved slightly higher CEs in the I-electrolyte cell than its control-counterpart, in the first 40 cycles (Figure 3b and Figure S4). As I_3^- consumed, the CEs of the I-electrolyte cell become slightly lower than the counterpart (98.83 vs. 98.94 % in average), but is still comparable with the volumes reported in literature.[1b,38] These results ascribe the improved striping/plating stability of Zn anodes to the I_3^- species in the initial I-electrolyte, rather than their reduced product I^-.

As reported, there are inevitably some manufacturing-induced imperfections on the surface of Zn foil electrodes, such as microcracks, scratches, fold lines, and unpolished cutting edges.[41] He and Huang's enlightening works convincingly show that these imperfections are always the nucleation and growth hotspots of Zn dendrites.[41] The reactions between I_3^- and Zn may passivate these hotspots, which possess high specific surface area and also high reactivity,[34] resulting in an obviously improved cycling durability (Figure 3c). In addition, the passivating effect further modified the morphology of the formed $Zn_4(OH)_6SO_4 \cdot H_2O$ layer, which may also contribute to stabilizing Zn anodes as chemically inert over layers.[13,16, 39] Compared with the traditional mechanical polishing process, this electrolyte-passivating method should be more convenient, since the former is difficult to treat cutting edges of micron-thick thin Zn foils. These results are in good line with above-mentioned hypothesis.

To further investigate the influence of the I_3^- species, the optical micrographs of the Zn electrodes are in situ collected during Zn plating (Figure 3d, e). In both electrolytes, the Zn deposit layers are almost bubble-free at the beginning. However, in the control-electrolyte, numerous bubbles are detected on the surface of the Zn electrode after 50 min Zn plating, indicating the occurrence of dynamic H_2 evolution reaction.[1b] This reaction is always accompanied by the corrosion of Zn, which in consequence accelerates Zn dendrite growth.[16,31] In the I-electrolyte, the H_2 evolution reaction is obviously suppressed by the competitive reactions between I_3^- and Zn [Eq. (1)], as shown by the much evolution rate of bubbles and the fading of the background maroon color from the I_3^- additive. Different from electrochemically inert corrosion product $Zn_4(OH)_6SO_4 \cdot H_2O$ in the control-electrolyte, the I_3^--oxidized ZnI_2 in the I-electrolyte should be reusable due to its high solubleness, and thus can further contribute capacities in subsequent cycling.[34–35] It is worth noting that this beneficial

process is persistent in full batteries, since the I^- can be re-oxidized into I_3^- on the cathode side. Therefore, this feature has been ingeniously used in Li-metal batteries to retrieve and rejuvenate the trapped Li species in both dead Li dendrites (i.e., electrically isolated Li debris) and discarded SEI, by converting them into solvable Li^+.[35]

The distinguishing data of the Zn/Zn symmetric cells motivate us to further verify the influence of I_3^- additives in full batteries. The full batteries employ a well-dispersed and high-performance carbon nanotube/α-MnO_2 (CNT/α-MnO_2, CNT content = 19%) composite as cathode material (Figure S5), via co-precipitation preparation.[39,42] This design can effectively suppress the cathode's distraction on the performance of the full cells, and thus clearly reflecting influences of the I_3^- additive.[43] As shown in Figure 4a, there are two pair of cathodic and anodic peaks at 1.39/1.22 and 1.54/1.58 V in the CV curves of both batteries, indicating a two-step redox process possibly relating to successive H^+ and Zn^{2+} insertion-extraction.[44] At a slow scan rate of 0.1 mV s^{-1}, the I-electrolyte battery manifests smaller CV peaks than the control-battery, indicating a lower capacity. Nevertheless, the intensity of I-electrolyte battery's CV peaks grows quickly with the increase of scanning rate, suggesting a better rate capability. At scanning rate > 0.5 mV s^{-1}, the capacity of I-electrolyte battery becomes dominant (Figure S6), thanks to the larger capacity contribution from ionic diffusion process (Figure 4b–d and S7). These CV results indicate that the introduction of I_3^- species is beneficial to the rate capability of batteries, probability due to the stabilized and uniform Zn striping/plating (Figure 4e).

Figure 4f further depicts the typical galvanostatic charge/discharge (GCD) curves of these two batteries at a current density of 1 A g^{-1}. In these curves, there are two voltage plateaus in both charge and discharge processes, corresponding well to the two step H^+/Zn^{2+} insertion/extraction processes.[44] The I-electrolyte battery delivers a reversible capacity of 160 mAh g^{-1}, 21% larger than that of the control-one (132 mAh g^{-1}). Under long-term cycling test (Figure 4g), the control-battery's capacity keeps relatively stable within the first 200 cycles, and then undergoes rapid capacity fading down to 73 mAh g^{-1} within the 200 ~ 400 cycles, corresponding to a capacity retention of ~55%. Between 566 and 800 cycles, the control-battery further suffers from serious capacity fluctuation, probability due to the soft short-circuit failure caused by the recoverable local internal contact.[16] In contrast, the capacity of the I-electrolyte battery gradually increases up to ~185 mAh g^{-1} after 30 cycles, and enjoys much slower fading within the testing period of 1200 cycles (Figure S8). Even at the end of cycling test, the battery still delivers a significant capacity of 147 mAh g^{-1}. The much-improved capacity and cycling stability of ZIBs are also detected at the current density of 500 mA g^{-1} (Figure S9), convincingly demonstrating the beneficial influence of I_3^- species in the electrolyte. The lower coulombic efficiencies of the I-electrolyte battery may stem from the I_3^--shuttle-derived self-discharge, as in the case of Zn-I_2 batteries.[23b,45] In addition, we further construct I-electrolyte

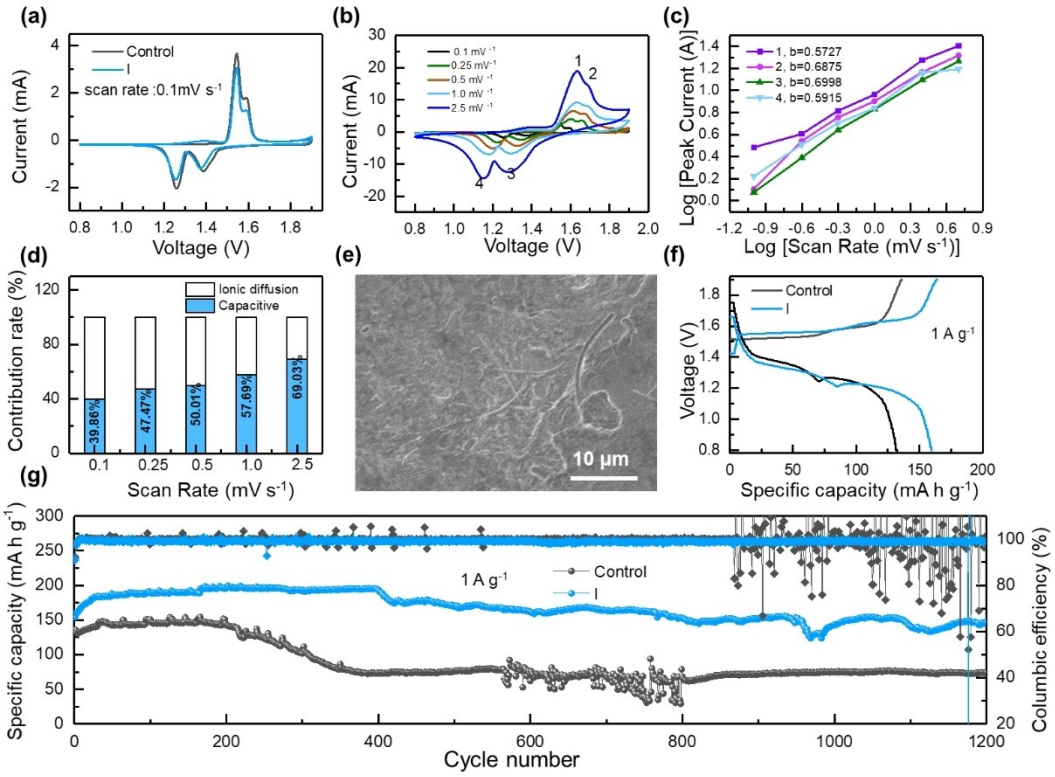

Figure 4. Electrochemical behaviors of full batteries with different electrolyte: a) cyclic voltammetry (CV) curves, b) CV curves at different scan rates in the I-electrolyte, c) linear fitting of the logarithm of peak current and sweeping rate, d) calculated capacity contributions from ionic diffusion and capacitive processes, e) SEM images of Zn anodes after 1200 cycles in full batteries, f) GCD curves and g) cycling performance.

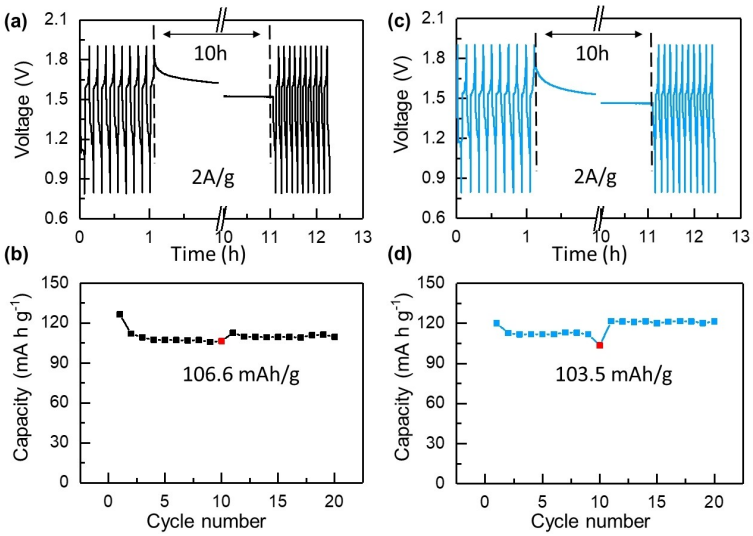

Figure 5. Galvanostatic cycling and self-discharge tests of Zn/MnO_2 batteries with either a, b) control- or c, d) I-electrolyte at a current density of 2 A g^{-1}.

Zn/MnO_2 batteries with higher mass loading of cathode active material. With a mass loading of 4.17 mg cm^{-2}, the battery is still decent in both capacity and cycling stability (Figure S10a). Further increasing the loading mass of cathode material results in high-density cracks and neglectable capacities, owing to the weak electrical connection between the active material layer and the current collector (Figure S10b). Figure S11 depicts the rate capability of full batteries with different electrolytes. It is clearly found that the I-electrolyte battery possesses much better rate performance in all the measured current densities from 2 to 0.2 A g^{-1}.

To further explore the influence of I_3^--additive on the self-discharge behaviors of these batteries, an open-circuit resting process was deliberately introduced into a normal GCD cycling test procedure. As shown in Figure 5a, b, the control-battery delivers a stable discharge capacity of ~107 mAh g^{-1} within the first 10 cycles. After 10 h of open-circuit resting, the capacity keeps almost unchanged. The I-electrolyte battery, on the other hand, delivers a slightly higher initial capacity of ~111 mAh g^{-1}, which slightly decreases down to 103.5 mAh g^{-1} after 10 h rest (Figure 5c, d). The lost capacity is recoverable by further charging, which can therefore mitigate the detrimental influence of I_3^--derived self-discharge in practical applications.[35]

3. Conclusion

We systematically investigate the influences of the I_3^- electrolyte additive on the performance of Zn anodes and Zn/MnO_2 full batteries. It is found that the addition of I_3^- can effectively prolong the striping/plating stability of the metallic Zn electrodes by oxidizing and passivating the growth hotspots of Zn dendrites. Furthermore, the oxidization of Zn by I_3^- can reduce the H_2 evolution and Zn corrosion rate, as it is competitive with the H_2O-derived parasitic reactions. The beneficial effects of the I_3^- addition is highly reproducible and more persistent in Zn/MnO_2 full batteries, thanks to the regeneration of I_3^- from I^- on the cathode side. Unfortunately, this additive cannot evolve into dense interfacial protect layer, and thus show marginal influences on avoiding long-term Zn lose. In our opinion, this strategy may find its value as a supplementary measure to prevent shorting failure of Zn-based batteries.

Experimental Section

Preparation of CNT/MnO_2 composite material

Firstly, high-performance CNT/MnO_2 composite cathode material was synthesized according to literature.[39,42] Before preparation, the CNTs (Shenzhen Nanotech Port Co., Ltd.) were purified by 68 wt.% HNO_3 (1.5 g in 50 mL) at 120 °C for 12 h in a Teflon-lined autoclave. This treatment also improved hydrophilicity and MnO_2 affinity of the CNTs by forming oxygen-containing interfacial groups, such as carbonyl, carboxyl and hydroxyl group, and therefore is favorable for the formation of well-dispersed MnO_2/CNT composite.[39,42] The acid-treated CNTs were washed with deionized water for 3 times by centrifugation, and then dried at 80 °C for 12 h.

To prepare the CNT/MnO_2 composite, 0.25 g acid-treated CNTs were dispersed in 20 mL, 0.3 M (i.e., mol L^{-1}) $Mn(CH_3COO)_2 \cdot 4H_2O$ aqueous solution by 30 min ultrasonication. Afterwards, 80 mL, 0.06 M $KMnO_4$ solution was mixed with the above CNTs–$Mn(CH_3COO)_2$ solution by 30 min stirring. The resulting solution was further heated at 80 °C for 6 h under continuous magnetic stirring. After naturally cooling to room temperature, the black CNT/MnO_2 precipitation was washed 3 times with deionized water, and finally dried at 80 °C for 12 h.

Fabrication of Zn/MnO_2 full batteries

The obtained CNT/MnO_2 composite (as cathode active material) was uniformly mixed with acetylene black (conductive additive) and polyvinylidene fluoride (PVDF, binder) with a weight ratio of 7:2:1. Afterwards, proper amount of 1-Methyl-2-pyrrolidinone (NMP) was added into the mixture under grinding, in order to obtain cathode coating slurry. The slurry was coated onto carbon papers (current collector) and dried at 60 °C for 12 h. The mass loading of active material on carbon papers was ~2.0 mg cm^{-2}.

Zn/MnO_2 full batteries in coin form were assembled with CNT/MnO_2 cathodes ($\phi = 16$ mm), glass fiber separators ($\phi = 19$ mm), metallic Zn foil anodes ($\phi = 16$ mm, 20 μm in thickness), and different electrolytes in a CR2032 coin cell form.

For the sake of comparison, a 2 M $ZnSO_4 + 0.2$ M $MnSO_4$ aqueous solution, labeled as control-electrolyte in the main text, was used as the baseline electrolyte of the full batteries. To introduce I_3^- anions into the electrolyte, 25 mM KI + 25 mM I_2 were added into the baseline electrolyte under 6 h stirring. After 1 h static standing, the supernatant was collected and used as I_3^--containing electrolyte (labeled as I-electrolyte in the main text).

Fabrication of Zn/Zn and Zn/Cu cells

To explore the I_3^--additives on the performances of Zn anodes while excluding the potential influence from cathode materials, Zn/Zn symmetric cells were assembled with Zn foils as both working and counter electrode. The employed electrolytes are the same as those used in the Zn/MnO_2 full batteries, except for the absence of $MnSO_4$ component. To determine Zn striping/plating coulombic efficiencies, Zn/Cu cells were also assembled with Cu and Zn foils as working and counter electrode, respectively.

Materials characterization

The surficial morphology and elemental mapping images of the samples was collected by a JEOL JSM-7610F field emission scanning electron microscope (SEM). X-ray powder diffraction (XRD) analyses were carried out on a D/max-2500/PC X-ray diffractometer with Cu Kα radiation ($\lambda = 0.1542$ nm). UV-vis absorption spectra of electrolytes were measured by a Cary 5000 UV-Vis-NIR spectrophotometer. Before testing, the electrolytes were diluted with water at a volume ratio of 1 : 100 to get a proper concentration. Contact angles of different electrolytes on the Zn foil anodes were determined by a Innuo CA100C static contact angle goniometer. The Zn electroplating behaviors on Zinc anodes were in situ observed using a ZEISS Stemi 508 optical microscope. The CNTs content in the CNT/MnO_2 composite was determined on a Netzsch STA 449 F3 thermogravimetric analyzer in air. Raman spectra were collected on a LabRAM HR Evolution Raman spectroscope with a 532 nm laser as light source. A JEOL-2100F field-emission transmission electron microscope (TEM) was employed to record TEM images.

Electrochemical characterization

Galvanostatic charge/discharge (GCD) tests were conducted in the voltage range of 0.8-1.9 V on Land CT2001 A battery test systems at different current densities and different capacities. Coulombic efficiencies (CEs) were also determined on Land CT2001 A battery test systems in a Zn/Cu cell configuration. Cyclic voltammetry (CV), curves were recorded by a CHI 660E electrochemical workstation.

Acknowledgements

The authors thank the National Natural Science Foundation of China (51502194, 51772257, 52072328), the Natural Science Foundation of Shandong (ZR2020ME024), the Major Basic Research Projects of Shandong Natural Science Foundation (ZR2018ZC1459) for financial support.

Conflict of Interest

The authors declare no conflict of interest.

Keywords: Zn · aqueous battery · I_3^- · electrolyte additive · dendrite

[1] a) T. C. Li, D. L. Fang, J. T. Zhang, M. E. Pam, Z. Y. Leong, J. Z. Yu, X. L. Li, D. Yan, H. Y. Yang, *J. Mater. Chem. A* **2021**, *9*, 6013–6028; b) Y. Z. Chu, S. Zhang, S. Wu, Z. L. Hu, G. L. Cui, J. Y. Luo, *Energy Environ. Sci.* **2021**, *14*, 3609–3620; c) L. E. Blanc, D. Kundu, L. F. Nazar, *Joule* **2020**, *4*, 771–799.
[2] H. Kim, G. J. Jeong, Y. U. Kim, J. H. Kim, C. M. Park, H. J. Sohn, *Chem. Soc. Rev.* **2013**, *42*, 9011–9034.
[3] L. T. Kang, M. W. Cui, Z. T. Zhang, F. Y. Jiang, *Batteries and Supercaps* **2020**, *3*, 966–1005.
[4] A. Naveed, H. J. Yang, Y. Y. Shao, J. Yang, N. Yanna, J. Liu, S. Q. Shi, L. W. Zhang, A. J. Ye, B. He, J. L. Wang, *Adv. Mater.* **2019**, *31*, 1900668.
[5] a) S. D. Han, N. N. Rajput, X. H. Qu, B. F. Pan, M. N. He, M. S. Ferrandon, C. Liao, K. A. Persson, A. K. Burrell, *ACS Appl. Mater. Interfaces* **2016**, *8*, 3021–3031; b) K. Ta, K. A. See, A. A. Gewirth, *J. Phys. Chem. C* **2018**, *122*, 13790–13796.
[6] Y. Dong, S. L. Di, F. B. Zhang, X. Bian, Y. Y. Wang, J. Z. Xu, L. B. Wang, F. Y. Cheng, N. Zhang, *J. Mater. Chem. A* **2020**, *8*, 3252–3261.
[7] a) D. Kundu, B. D. Adams, V. Duffort, S. H. Vajargah, L. F. Nazar, *Nat. Energy* **2016**, *1*, 16119; b) K. W. Nam, H. Kim, J. H. Choi, J. W. Choi, *Energy Environ. Sci.* **2019**, *12*, 1999–2009; c) F. Wang, W. Sun, Z. Shadike, E. Y. Hu, X. Ji, T. Gao, X. Q. Yang, K. Xu, C. S. Wang, *Angew. Chem. Int. Ed.* **2018**, *57*, 11978–11981; *Angew. Chem.* **2018**, *130*, 12154–12157; d) D. H. Wang, L. F. Wang, G. J. Liang, H. F. Li, Z. X. Liu, Z. J. Tang, J. B. Liang, C. Y. Zhi, *ACS Nano* **2019**, *13*, 10643–10652.
[8] A. Naveed, H. J. Yang, J. Yang, Y. Nuli, J. L. Wang, *Angew. Chem. Int. Ed.* **2019**, *58*, 2760–2764; *Angew. Chem.* **2019**, *131*, 2786–2790.
[9] N. Zhang, M. Jia, Y. Dong, Y. Y. Wang, J. Z. Xu, Y. C. Liu, L. F. Jiao, F. Y. Cheng, *Adv. Funct. Mater.* **2019**, *29*, 1807331.
[10] a) J. Huang, J. D. Liu, J. He, M. G. Wu, S. H. Qi, H. P. Wang, F. Li, J. M. Ma, *Angew. Chem. Int. Ed. Engl.* **2021**, *60*, 20717–20722; b) F. Li, J. He, J. D. Liu, M. G. Wu, Y. Y. Hou, H. P. Wang, S. H. Qi, Q. H. Liu, J. W. Hu, J. M. Ma, *Angew. Chem. Int. Ed. Engl.* **2021**, *60*, 6600–6608.
[11] Z. M. Zhao, J. W. Zhao, Z. L. Hu, J. D. Li, J. J. Li, Y. J. Zhang, C. Wang, G. L. Cui, *Energy Environ. Sci.* **2019**, *12*, 1938–1949.
[12] J. N. Hao, X. L. Li, S. L. Zhang, F. H. Yang, X. H. Zeng, S. Zhang, G. Bo, C. S. Wang, Z. P. Guo, *Adv. Funct. Mater.* **2020**, *30*, 2001263.
[13] H. B. Yan, S. M. Li, Y. Nan, S. B. Yang, B. Li, *Adv. Energy Mater.* **2021**, *11*, 2100186.
[14] a) L. T. Ma, Q. Li, Y. R. Ying, F. X. Ma, S. M. Chen, Y. Y. Li, H. T. Huang, C. Y. Zhi, *Adv. Mater.* **2021**, *33*, 2007406; b) Y. L. An, Y. Tian, K. Zhang, Y. P. Liu, C. K. Liu, S. L. Xiong, J. K. Feng, Y. T. Qian, *Adv. Funct. Mater.* **2021**, *31*, 2101886.
[15] J. N. Hao, B. Li, X. L. Li, X. H. Zeng, S. L. Zhang, F. H. Yang, S. L. Liu, D. Li, C. Wu, Z. P. Guo, *Adv. Mater.* **2020**, *32*, 2003021.
[16] L. Zhang, B. Zhang, T. Zhang, T. Li, T. F. Shi, W. Li, T. Shen, X. X. Huang, J. J. Xu, X. G. Zhang, Z. Y. Wang, Y. L. Hou, *Adv. Funct. Mater.* **2021**, *31*, 2100186.
[17] H. Jia, Z. Q. Wang, B. Tawiah, Y. D. Wang, C. Y. Chan, B. Fei, F. Pan, *Nano Energy* **2020**, *70*, 104523.
[18] D. Li, L. Cao, T. Deng, S. Liu, C. Wang, *Angew. Chem. Int. Ed. Engl.* **2021**, *60*, 13035–13041.
[19] P. He, J. X. Huang, *ACS Energy Lett.* **2021**, *6*, 1990–1995.
[20] S. H. Qi, H. P. Wang, J. He, J. D. Liu, C. Y. Cui, M. G. Wu, F. Li, Y. Z. Feng, J. M. Ma, *Sci. Bull.* **2021**, *66*, 685–693.
[21] F. Wang, O. Borodin, T. Gao, X. L. Fan, W. Sun, F. D. Han, A. Faraone, J. A. Dura, K. Xu, C. S. Wang, *Nat. Mater.* **2018**, *17*, 543–549.
[22] J. W. Zhao, J. Zhang, W. H. Yang, B. B. Chen, Z. M. Zhao, H. Y. Qiu, S. M. Dong, X. H. Zhou, G. L. Cui, L. Q. Chen, *Nano Energy* **2019**, *57*, 625–634.
[23] a) Q. Han, X. W. Chi, S. M. Zhang, Y. Z. Liu, B. Zhou, J. H. Yang, Y. Liu, *J. Mater. Chem. A* **2018**, *6*, 23046–23054; b) W. Shang, J. Zhu, Y. Liu, L. Kang, S. Liu, B. Huang, J. Song, X. Li, F. Jiang, W. Du, Y. Gao, H. Luo, *ACS Appl. Mater. Interfaces* **2021**, *13*, 24756–24764.
[24] Q. Zhang, J. Y. Luan, L. Fu, S. G. Wu, Y. G. Tang, X. B. Ji, H. Y. Wang, *Angew. Chem. Int. Ed.* **2019**, *131*, 15988–15994.

[25] a) A. Bayaguud, X. Luo, Y. P. Fu, C. B. Zhu, *ACS Energy Lett.* **2020**, *5*, 3012–3020; b) F. Wan, L. Zhang, X. Dai, X. Y. Wang, Z. Q. Niu, J. Chen, *Nat. Commun.* **2018**, *9*, 1656.
[26] a) N. Zhang, F. Y. Cheng, Y. C. Liu, Q. Zhao, K. X. Lei, C. C. Chen, X. S. Liu, J. Chen, *J. Am. Chem. Soc.* **2016**, *138*, 12894–12901; b) B. Wang, M. W. Cui, Y. F. Gao, F. Y. Jiang, W. Du, F. Gao, L. T. Kang, C. Y. Zhi, H. J. Luo, *Solar RRL* **2020**, *4*, 1900425; c) C. X. Li, W. T. Yuan, C. Li, H. Wang, L. B. Wang, Y. C. Liu, N. Zhang, *Chem. Commun.* **2021**, *57*, 4319–4322.
[27] a) L. S. Cao, D. Li, E. Y. Hu, J. Xu, T. Deng, L. Ma, Y. Wang, X. Q. Yang, C. S. Wang, *J. Am. Chem. Soc.* **2020**, *142*, 21404–21409; b) Q. S. Nian, X. R. Zhang, Y. Z. Feng, S. Liu, T. J. Sun, S. B. Zheng, X. D. Ren, Z. L. Tao, D. H. Zhang, J. Chen, *ACS Energy Lett.* **2021**, *6*, 2174–2180.
[28] a) R. Z. Qin, Y. T. Wang, M. Z. Zhang, Y. Wang, S. X. Ding, A. Song, H. C. Yi, L. Y. Yang, Y. L. Song, Y. H. Cui, J. Liu, Z. Q. Wang, S. N. Li, Q. H. Zhao, F. Pan, *Nano Energy* **2021**, *80*, 105478; b) V. Verma, R. M. Chan, L. Jia Yang, S. Kumar, S. Sattayaporn, R. Chua, Y. Cai, P. Kidkhunthod, W. Manalastas, M. Srinivasan, *Chem. Mater.* **2021**, *33*, 1330–1340.
[29] Y. Dong, L. C. Miao, G. Q. Ma, S. L. Di, Y. Y. Wang, L. B. Wang, J. Z. Xu, N. Zhang, *Chem. Sci.* **2021**, *12*, 5843–5852.
[30] W. N. Xu, K. N. Zhao, W. C. Huo, Y. Z. Wang, G. Yao, X. Gu, H. W. Cheng, L. Q. Mai, C. G. Hu, X. D. Wang, *Nano Energy* **2019**, *62*, 275–281.
[31] X. H. Zeng, J. F. Mao, J. N. Hao, J. T. Liu, S. L. Liu, Z. J. Wang, Y. Y. Wang, S. L. Zhang, T. Zheng, J. W. Liu, P. H. Rao, Z. P. Guo, *Adv. Mater.* **2021**, *33*, 2007416.
[32] J. Z. Ma, M. M. Liu, Y. L. He, J. T. Zhang, *Angew. Chem. Int. Ed.* **2021**, *60*, 12636–12647.
[33] X. L. Li, M. Li, Z. D. Huang, G. J. Liang, Z. Chen, Q. Yang, Q. Huang, C. Y. Zhi, *Energy Environ. Sci.* **2021**, *14*, 407–413.
[34] C. X. Xie, H. M. Zhang, W. B. Xu, W. Wang, X. F. Li, *Angew. Chem. Int. Ed.* **2018**, *57*, 11171–11176; *Angew. Chem.* **2018**, *130*, 11341–11346.
[35] C. B. Jin, T. F. Liu, O. W. Sheng, M. Li, T. C. Liu, Y. F. Yuan, J. W. Nai, Z. J. Ju, W. K. Zhang, Y. J. Liu, Y. Wang, Z. Lin, J. Lu, X. Y. Tao, *Nat. Energy* **2021**, *6*, 378–387.
[36] L. T. Ma, Y. R. Ying, S. M. Chen, Z. D. Huang, X. L. Li, H. T. Huang, C. Y. Zhi, *Angew. Chem. Int. Ed.* **2021**, *60*, 3791–3798; *Angew. Chem.* **2021**, *133*, 3835–3842.
[37] Q. Yang, Q. Li, Z. X. Liu, D. H. Wang, Y. Guo, X. L. Li, Y. C. Tang, H. F. Li, B. B. Dong, C. Y. Zhi, *Adv. Mater.* **2020**, *32*, 2001854.
[38] S. Y. Li, J. Fu, G. X. Miao, S. P. Wang, W. Y. Zhao, Z. C. Wu, Y. J. Zhang, X. W. Yang, *Adv. Mater.* **2021**, *33*, 2008424.
[39] L. T. Kang, M. M. Cui, F. Y. Jiang, Y. F. Gao, H. J. Luo, J. J. Liu, W. Liang, C. Y. Zhi, *Adv. Energy Mater.* **2018**, *8*, 1801090.
[40] J. Y. Ding, Y. Liu, S. Z. Huang, X. S. Wang, J. F. Yang, L. J. Wang, M. Q. Xue, X. X. Zhang, J. T. Chen, *ACS Appl. Mater. Interfaces* **2021**, *13*, 29746–29754.
[41] P. He, J. X. Huang, *ACS Energy Lett.* **2021**, *6*, 1990–1995.
[42] D. W. Xu, B. H. Li, C. G. Wei, Y. B. He, H. D. Du, X. D. Chu, X. Y. Qin, Q. H. Yang, F. Y. Kang, *Electrochim. Acta* **2014**, *133*, 254–261.
[43] J. T. Hu, B. B. Wu, S. J. Chae, J. Lochala, Y. J. Bi, J. Xiao, *Joule* **2021**, *5*, 1011–1015.
[44] W. Sun, F. Wang, S. Hou, C. Y. Yang, X. L. Fan, Z. H. Ma, T. Gao, F. D. Han, R. Z. Hu, M. Zhu, C. S. Wang, *J. Am. Chem. Soc.* **2017**, *139*, 9775–9778.
[45] W. Li, K. L. Wang, K. Jiang, *J. Mater. Chem. A* **2020**, *8*, 3785–3794.

Manuscript received: August 18, 2021
Revised manuscript received: September 22, 2021
Accepted manuscript online: September 26, 2021
Version of record online: October 19, 2021